KINEMATICS OF GAS AND STARS IN 20 DISC GALAXIES

J.C. VEGA BELTRÁN
TNG, Osservatorio Astronomico di Padova, vicolo dell'Osservatorio 5, I-35122 Padova, Italy
E-mail: jvega@ll.iac.es

W.W. ZEILINGER
Institute fur Astronomie, Universitat Wien, Wien, Austria
E-mail: zeilinger@astro.univie.ac.at

A. PIZZELLA
European Southern Observatory, Santiago 19, Chile
E-mail: apizzell@eso.org

E.M. CORSINI, F. BERTOLA and J.G. FUNES
Dipartimento di Astronomia, Università di Padova, vicolo dell'Osservatorio 5, I-35122 Padova, Italy
E-mail: corsini@pd.astro.it; bertola@pd.astro.it; funes@pd.astro.it

J.E. BECKMAN
Instituto de Astrofísica de Canarias, E-38200 La laguna, Tenerife, Spain
E-mail: jeb@ll.iac.es

Abstract. In this paper we present the kinematics of the gas and/or the stars of a sample of 20 disc galaxies. We investigate whether there is any relation between the kinematics of the gas and stars and the classical morphological type of the galaxies in the sample. We deduce that, in most of the late-type spirals we have studied, the stars and the ionized gas are moving with virtually circular velocity, except when the spectroscopic slit crosses a bar region. On the other hand, we found in the central parts of early-type disc galaxies a wider variety of different behaviour of stars and gas. We find many possible factors that complicate the classification of the kinematical properties of the galaxies by their morphological type: the presence of counter-rotations (star vs. stars or star vs. gas), misalignment between the different kinematic components present in the galaxy, the presence of a bar structure and its orientation with respect to the line of nodes of the galaxy, and interactions and mergers or external accretion processes are some of the problems we find in the study of the kinematics of a galaxy.

1. Introduction

The main body of the spectroscopic observations used in this contribution belongs to a long term programme whose primary goal is to make a statistical comparison study between the gas and the stellar kinematics of the sample and analyse if there is any correlation between kinematics and morphologic classification in disc galaxies.

Astrophysics and Space Science **276:** 1201–1210, 2001.

We have seen that stellar spectra can give a lot of information about the movement of the stars in a galaxy; the same is clearly true of the gas spectra with respect to the gas, but it is of special interest to make a comparison between the kinematics of the gas and the stars. This study will show a wide variety of cases of comparisons between the kinematics of gas and stars for the galaxies in the sample: gas rotating more quickly than. at the same velocity as, and sometimes more slowly than the stars, and the increasingly frequently observed phenomenon of stellar counter-rotation (see Corsini and Bertola, 1998). We have tried to give an explanation for the kinematics of each galaxy; sometimes the interpretation was not unique because of the limitations of the available observational data. In these cases, we will need new spectroscopic observations (higher S/N, either at higher spectral or spatial resolution, or a more complete velocity field) to resolve the dichotomy in the interpretation of the kinematics.

2. Observations and Data Reduction

The long-slit spectroscopic observations of the sample of galaxies we present in this paper were carried out at the 1.52 m ESO Telescope at La Silla, at the 2.5 m Isaac Newton Telescope (INT) on La Palma and at the 4.5 m MMT in Arizona. In Table I we give some general parameters for every galaxy of the sample studied.

In this section we enumerate the whole sample of the galaxies to be studied and we describe the different spectroscopic runs of observations taken to complete this sample. We also give a brief description of the data reduction process for each run of observation. In Table II we summarize the general set-up configuration of the different runs. For all the objects we have our own spectroscopic data (gas and stellar kinematics).

Now we give a general introduction of the data reduction process.

2.1. General spectroscopic data reduction process

The standard spectral reduction was performed by using the ESO-MIDAS⋆ package. All the spectra were bias-subtracted, flat-field corrected by quartz lamp exposures and wavelength calibrated by fitting the position of the comparison lines with cubic polynomials. Pixels affected by cosmic-ray events were identified and then corrected. The contribution of the night sky was determined from the edge regions (not contaminated by galaxy light) of each spectrum and then subtracted.

The galaxies were centred on the slit using the guiding camera at the beginning of each exposure. Spectra of late G- or early K-giant stars were obtained to serve as templates in measuring the stellar kinematics. Comparison lamp exposures were obtained before and after each object integration. The stellar kinematics was

⋆ MIDAS is developed and maintained by the European Southern Observatory.

TABLE I

Parameters of the sample galaxies

Object [name] (1)	Type [RSA] (2)	B_T [mag] (3)	P.A. [°] (4)	i [°] (5)	$V_\odot$ [km s^{-1}] (6)	V_0 [km s^{-1}] (7)	D [Mpc] (8)	Scale [pc$''^{-1}$] (9)
NGC 224	Sb	4.36	35	72	-290 ± 10	50	0.7	3
NGC 470	Sbc(s)	12.53	135	52	2370 ± 10	2480	33.0	160
NGC 772	Sb(rs)	11.09	130	54	2470 ± 10	2620	34.7	168
NGC 949	Sc(s)	12.40	145	58	620 ± 10	785	10.5	51
NGC 980	...	...	110	58	5765 ± 10	5936	79.1	384
NGC 1160	...	13.50	50	62	2510 ± 10	2765	36.9	179
NGC 2541	Sc(s)	12.26	165	61	565 ± 10	610	8.1	39
NGC 2683	Sb	10.64	44	78	400 ± 10	358	4.8	23
NGC 2841	Sb	10.09	147	65	640 ± 10	690	9.2	45
NGC 3031	Sb(r)	7.89	157	59	-50 ± 10	90	1.2	6
NGC 3200	Sb(r)	12.83	169	73	3550 ± 10	3299	44.0	213
NGC 3368	Sab(s)	10.11	5	47	865 ± 10	732	9.8	47
NGC 3705	Sab(r)	11.86	122	66	1000 ± 10	875	11.7	57
NGC 3810	Sc(s)	11.35	15	45	1000 ± 10	890	11.9	58
NGC 3898	Sa	11.60	107	54	1184 ± 10	1283	17.1	83
NGC 4419	SBab:	12.08	133	71	-195 ± 5	-255	17	82
NGC 5064	Sa	12.75	38	64	2980 ± 10	2750	36.7	178
NGC 5854	Sa	12.71	55	80	1630 ± 10	1636	21.8	106
NGC 7331	Sb(rs)	10.35	171	70	820 ± 10	1100	14.7	71
NGC 7782	Sb(s)	13.08	175	58	5430 ± 10	5611	74.8	363

Col. (2): classification from RSA (Sandage and Tammann, 1981). Col. (3): total observed blue magnitude from RC3 except for NGC 5064 (Tully, 1988) Col. (4): major-axis position angle taken from RC3. Col. (5): inclination derived with the Hubble's (1926) formula $\cos^2 i = (q^2 - q_0^2)/(1 - q_0^2)$. The observed axial ratio, q, is taken from RC3 and the intrinsic flattening, $q_0 = 0.11$, has been assumed following Guthrie (1992). Col. (6): heliocentric velocity of the galaxy derived as center of symmetry of the gas RC. Col. (7): systemic velocity derived from $V_\odot$ corrected for the motion of the Sun with respect of the Local Group by $\Delta V = 300 \cos b \sin l$. Col. (8): distance obtained as V_0/H_0 with $H_0 = 75$ km s^{-1} Mpc^{-1} except for NGC 4419. It belongs to the Virgo cluster for which we assume a distance of 17 Mpc (Freedman *et al.*, 1994).

measured from the absorption lines present in each spectrum using the Fourier correlation quotient method (Bender, 1990) as applied by Bender, Saglia and Gerhard (1994).

The ionized gas velocities and velocity dispersions were derived by means of MIDAS package ALICE. We measured the emission lines, where they were clearly detected. The position, the FWHM and the uncalibrated flux of each emission line were individually determined by interactively fitting a Gaussian to each emission

TABLE II
Observing set-up

Parameter	INT (2.5 m)	ESO (1.5 m)	MMT (3.5 m)
Date	1996 March	1992 May	1990 Oct–Dec
Spectrograph	IDS	BandC	Red Channel
Grism/grating (groove mm^{-1})	1800	1200	1200
Detector	TK1024A	FA2048L	12×8 mmt
Pixel size (μm^2)	24×24	15×15	15×15
Pixel binning	1×1	1×1	1×1
Scale ($''$ $pixel^{-1}$)	0.33	0.81	0.30
Reciprocal dispersion (Å $pixel^{-1}$)	0.24	0.98	0.82
Slit width ($''$)	1.9	2.5	1.3
Slit length ($'$)	4.0	2.1	3.0
Spectral range (Å)	6650–6890	4900–6900	4850–5450
Comparison lamp	Cu–Ar	He–Ar	He–Ne–Ar–Fe
Instrumental FWHM (Å)	0.869 ± 0.040	2.34 ± 0.09	2.5 ± 0.5
Instrumental σ at Hα (km s^{-1})	16.86 ± 0.78	44.20 ± 1.68	45 ± 5.0
Seeing FWHM ($''$)	1.0–1.8	1.0–1.5	1.2–1.5

plus a polynomial to its surrounding continuum. The wavelength of the Gaussian centre was converted into velocity via the optical convention $v = cz$, then the standard heliocentric correction was applied. The Gaussian FWHM was corrected for the instrumental FWHM and then converted into the velocity dispersion. At some radii, where the intensity of the emission lines was low, we averaged adjacent spectral rows to improve the signal-to-noise ratio.

3. Discussion and Results

In this section we present the kinematics and the photometry of some galaxies in the sample. The way in which we present the data is optimized to show clearly the correspondence between the kinematics and the photometry.

In the central regions of the late-type spirals we observe almost the same velocity gradient for both stars and gas ($\Delta V_\star/\Delta r \approx \Delta V_{\rm gas}/\Delta r$). The same is true for their velocity dispersions ($\sigma_\star \approx \sigma_{\rm gas}$), which are characterized by low values ($\sim$ 50 km s^{-1}) over the full observed radial range. As an example of this kind of kinematics, we show in Figure 1 the Scd galaxy NGC 1160. This is also the case for the late-types NGC 949 and NGC 2541. We deduce that in most of the late-type spirals we have studied the stars and the ionized gas are moving virtually at the circular velocity.

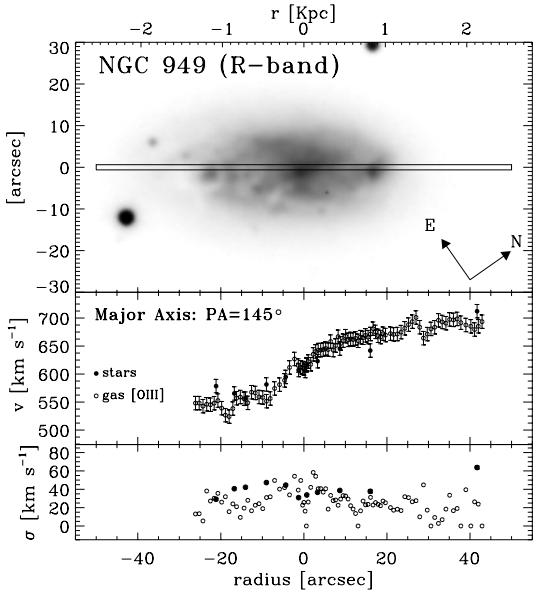

Figure 1. Major-axis kinematics of NGC 949.

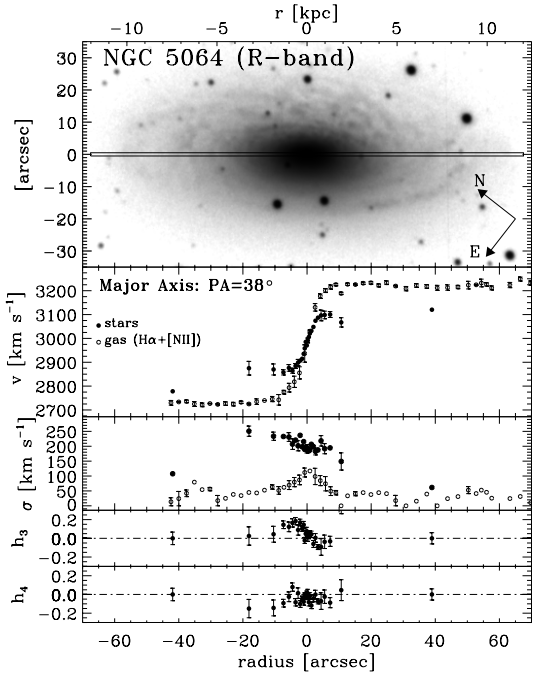

Figure 2. Major-axis kinematics of NGC 5064.

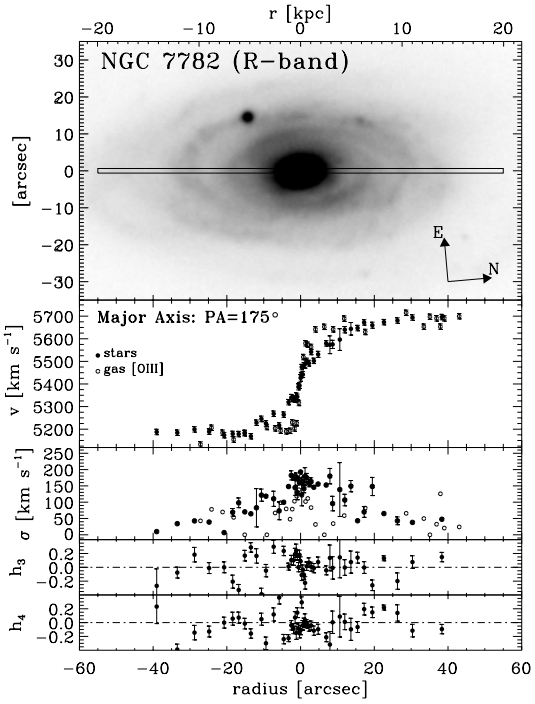

Figure 3. Major-axis kinematics of NGC 7782.

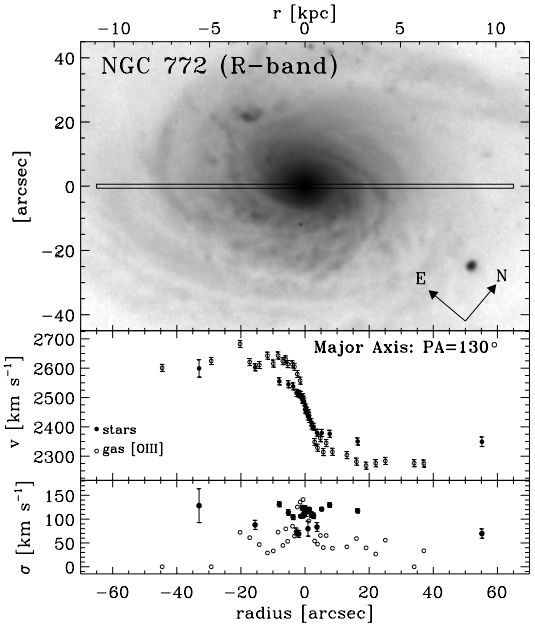

Figure 4. Major-axis kinematics of NGC 772.

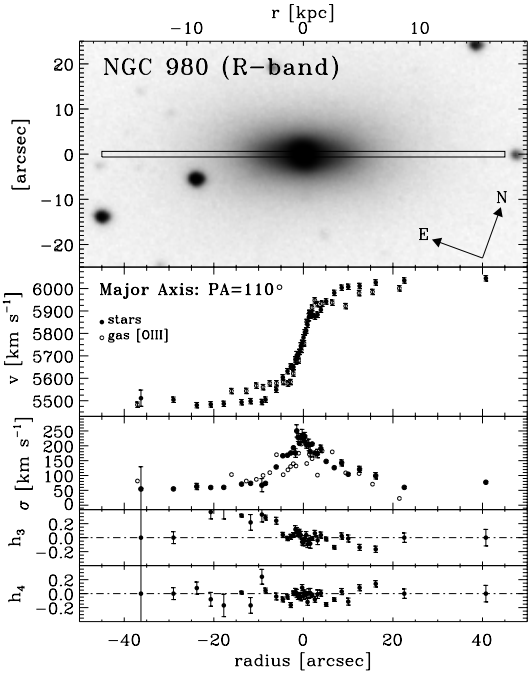

Figure 5. Major-axis kinematics of NGC 980.

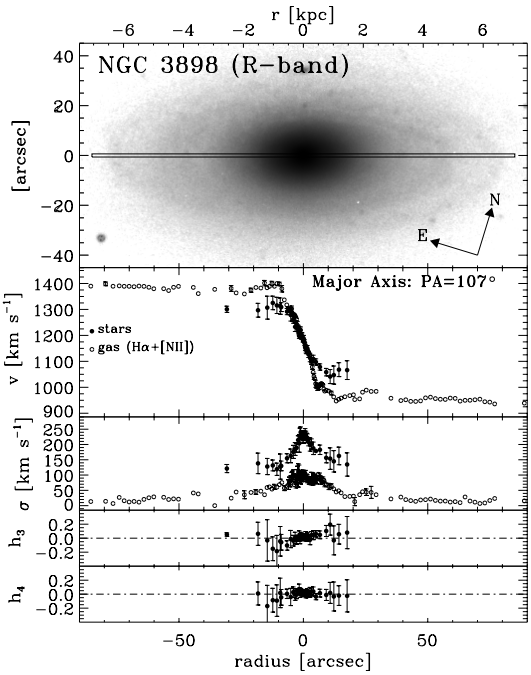

Figure 6. Major-axis kinematics of NGC 3898.

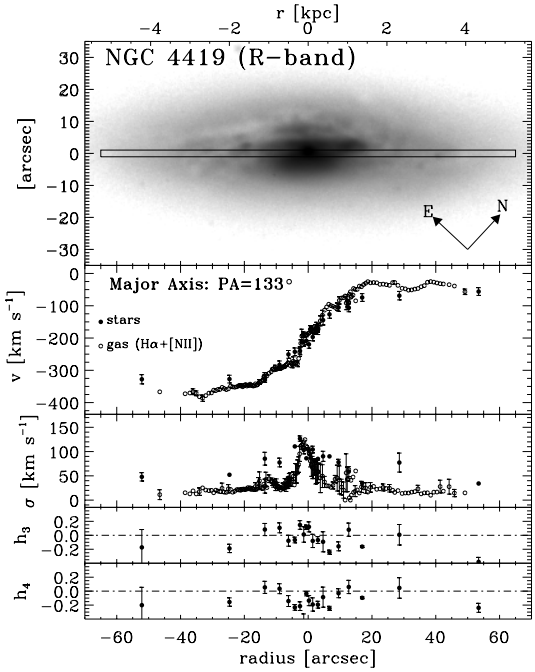

Figure 7. Major-axis kinematics of NGC 4419.

The central parts of early-type disc galaxies reveal a wider variety of different behaviour for the stars and gas. We generally find for stars and gas $\Delta V_\star/\Delta r < \Delta V_{\rm gas}/\Delta r$ and $\sigma_\star > \sigma_{gas} \sim 50$ km s^{-1} (e.g. NGC 5064—Figure 2, NGC 7782—Figure 3). This can be easily explained by considering that the stellar and gaseous kinematics are dominated by dynamical pressure and rotation, respectively. The observed stellar rotation can be corrected to that corresponding to the circular velocity traced by the gas rotation by including the asymmetric drift effect (see, for example, Binney and Tremaine, 1987, for a brief explanation).

In the early-type disc galaxies NGC 772, NGC 980 and NGC 3898, we derived $\Delta V_\star/\Delta r \approx \Delta V_{\rm gas}/\Delta r$ and we found $\sigma_\star \approx \sigma_{\rm gas} \geq 120$ km s^{-1} over an extended radial range. In Figures 4, 5 and 6 we show the radial dependence of the kinematics of the early-type galaxies NGC 772, NGC 980 and NGC 3898, respectively. The presence of a gaseous component with a high central velocity dispersion has been previously detected in the nuclei of lenticulars and early-type spirals by a number of authors (Fillmore, Boroson and Dressler, 1986; Kent, 1988; Kormendy and Westpfahl, 1989). This has been explained by Bertola *et al.* (1995) who showed that random motions are also crucial for the dynamical support of the gas, e.g. see the detailed model for NGC 4036 by Cinzano *et al.* (1999). The peculiar stellar and/or gaseous kinematics of the remaining early-type spirals of the sample is due to the presence of triaxial (e.g. NGC 4419–Figure 7) or counter-rotating (e.g. NGC 2841, NGC 7331–Figure 8) components. These components have been detected (even

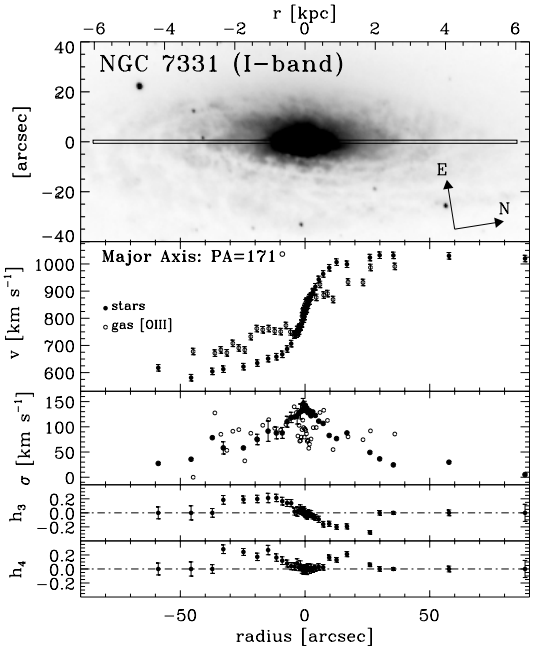

Figure 8. Major-axis kinematics of NGC 7331.

when they were photometrically unresolved) due to the hallmarks they leave in the observed kinematics, e.g. 'wavy pattern' rotation curves, 'figure-of-eight' rotation curves 'M-shaped' velocity dispersion profiles and asymmetries in h_3 profiles (see Vega Beltrán *et al.*, these proceedings).

In order to investigate quantitatively the relationship between the kinematics of stars and gas and the mass distribution of spirals we apply self-consistent dynamical models (Pignatelli and Galletta, 1998) to a subsample of the galaxies presented here. The models derive, from the stellar photometric data, the gravitational potential in which the ionized gas is expected to orbit. They take into account the asymmetric drift effects, the projection effects along the line of sight and the non-Gaussian shape of the line profiles due to the presence of different components with distinct dynamical behaviour. In Vega Beltrán *et al.* (these proceedings) we give a detailed treatment of the models and the obtained results.

References

Bender, R.: 1990, *Astron. Astrophys.* **229**, 441.

Bender, R., Saglia, R.P. and Gerhard, O.E.: 1994, *Mon. Not. R. Astron. Soc.* **307**, 433.

Bertola, F., Cinzano, P., Corsini, E.M., Rix, H.-W. and Zeilinger, W.W.: 1995, *Astrophys. J. Lett.* **448**, L13.

Binney, J. and Tremaine, S.: 1987, *Galactic Dynamics*, Princeton University Press, Princeton.

Cinzano, P., Rix, H.-W., Sarzi, M., Corsini, E.M., Zeilinger, W.W. and Bertola, F.: 1999, *Mon. Not. R. Astron. Soc.*, **307**, 433.
Corsini, E.M. and Bertola, F.: 1998, *J. Korean Phys. Soc.* **33**, 574.
Fillmore, J.A., Boroson, T.A. and Dressler, A.: 1986, *Astrophys. J.* **302**, 208.
Freedman, W.L., *et al.*: 1994, *Nature* **371**, 757.
Guthrie, B.N.G.: 1992, *Astron. Astrophys. Suppl.* **93**, 255.
Kent, S.M.: 1988, *Astron. J.* **96**, 514.
Kormendy, J. and Westpfahl, D.J.: 1989, *Astrophys. J.* **338**, 752.
Pignatelli, E. and Galletta, G.: 1998, *Astron. Astrophys.* **349**, 369.
Sandage, A. and Tammann, G.A.: 1981, *A Revised Shapley–Ames Catalog of Bright Galaxies*, Carnegie Institution, Washington DC (RSA).
Tully, R.B.: *Nearby Galaxies Catalog*, Cambridge University Press, Cambridge.